RSC Advances

COMMUNICATION

View Article Online
View Journal | View Issue

Polyvinyl pyrrolidone-assisted synthesis of a Fe_3O_4/graphene composite with excellent lithium storage properties†

Cite this: *RSC Adv.*, 2014, **4**, 6379

Received 21st October 2013
Accepted 23rd December 2013

DOI: 10.1039/c3ra45993d

www.rsc.org/advances

Mochao Cai, Hang Qian, Zhikai Wei, Jiajia Chen, Mingsen Zheng* and Quanfeng Dong*

This paper reports a weak interaction between metal oxide and graphene in the Fe_3O_4/graphene composite, which results in the superior electrochemical performance.

Carbon based composites with well-designed nanostructure have attracted considerable research activities and demonstrated improved electrochemical performance[1–8] for lithium ion batteries (LIBs). The carbon matrix in the composites can not only provide better electronic conductivity, but also buffer the volume expansion of active materials. For example, graphene nanosheets (GNS) have been widely used as a carbon matrix to prepare nanocomposite anodes for lithium ion batteries due to their high electronic conductivity,[9] prominent thermal stability,[10] remarkable structural flexibility and ultrahigh specific surface area.[11] Numerous graphene-based nanocomposites such as Co_3O_4/GNS,[12] α-Fe_2O_3/GNS,[13] MnO_2/GNS[14] and Fe_3O_4/GNS[15–18] have been synthesized and showed enhanced electrochemical performance. However, besides the abovementioned advantages, the interactions between metal oxide and the GNS matrix as well as the mechanism of the improvement are rarely reported.

As one of the most promising anode materials for LIBs, Fe_3O_4 has been intensively investigated owing to its low cost, resource abundance, environmental friendliness and high theoretical capacity of about 924 mA h g^{-1},[17–23] which is almost three times larger than that of commercial graphite anodes. Moreover, Fe_3O_4 exhibits better safety performance than graphite because no metallic lithium forms during the lithium insertion/extraction process. However, the relatively low electronic conductivity and large volume variation during charge–discharge process result in the pulverization and aggregation of the nanoparticles, and consequently poor electrochemical performance.

State Key Laboratory for Physical Chemistry of Solid Surfaces and Department of Chemistry, College of Chemistry and Chemical Engineering, Xiamen University, Xiamen, Fujian 361005, China. E-mail: qfdong@xmu.edu.cn

† Electronic supplementary information (ESI) available: Experimental procedures. See DOI: 10.1039/c3ra45993d

Herein, we report a novel and facile method to synthesize Fe_3O_4/GNS nanocomposites. Polyvinyl Pyrrolidone (PVP) was used as capping agent to protect nanoparticles from coagulation or precipitation.[24–27] The presence of PVP molecules[28] stabilized the graphene oxide suspension and facilitated the deposition of Fe_3O_4 nanoparticles on graphene. The as-prepared Fe_3O_4/graphene nanocomposite exhibited a large reversible capacity, significantly enhanced cycling performance and rate capability. The superior lithium storage properties are attributed not only to the well dispersion of Fe_3O_4 on GNS, but also the interaction between GNS and Fe_3O_4.

As shown in Fig. 1, we employed PVP as capping agent and surfactant to disperse graphene oxide and the resulting Fe_3O_4 nanoparticles. Many studies have focused on utilizing surfactant to control the growth and size distribution of nanoparticles.[29–31] The surfactant PVP contains hydrophobic methylene carbon chains and strong polar lactams in the molecule which can be adsorbed on the surface of nanoparticles.[32] The surfactant can form complexes with the precursors to control the reaction process and prevent the aggregation of nanoparticles. The composites prepared with or without the assistance of PVP were denoted as Fe_3O_4/GNS–PVP and Fe_3O_4/GNS, respectively. X-ray diffraction results demonstrated the successful preparation of the composites, and the

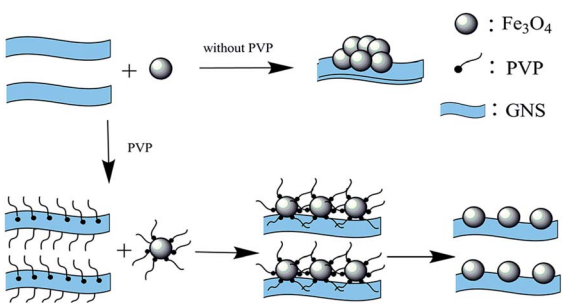

Fig. 1 Schematic illustration of the synthesis of Fe_3O_4 and GNS composites.

weight contents of Fe_3O_4 in Fe_3O_4/GNS–PVP and Fe_3O_4/GNS are about 78 wt% (ESI, Fig. S1b†).

The morphology of the Fe_3O_4/GNS–PVP and Fe_3O_4/GNS composites was investigated by TEM. Fig. 2a shows a TEM image of Fe_3O_4/GNS–PVP composite. The folding nature of graphene can be clearly observed. The particle size of Fe_3O_4 in the composite is about 25 nm. In addition, it should be noted that little agglomeration of Fe_3O_4 nanoparticles is observed and Fe_3O_4 nanoparticles are anchoring firmly on graphene surface considering the long time sonication during the preparation of TEM samples. Although the mass percentage of Fe_3O_4 in the composites is 78%, the graphene surface is not completely covered. The space between Fe_3O_4 nanoparticles would benefit the lithium ion diffusion and accommodates the volume expansion during the lithium insertion process, implying good cyclic stability and rate capability.[33] As a comparison, TEM image of the composite without the assistance of PVP is shown in Fig. 2b. It reveals that primary Fe_3O_4 nanoparticles aggregate into big clusters with particle size of several hundred nanometers.

The electrochemical performance of the as-prepared Fe_3O_4/GNS–PVP was investigated by galvanostatic charge–discharge method. Fig. 3a shows the discharge curves of the electrode for the first and second cycles at a current density of 0.1 A g^{-1} from 20 mV to 3.0 V *versus* Li^+/Li. A distinct voltage plateau is clearly observed at ~0.75 V corresponding to lithium insertion and Li_2O formation in the discharge process, which agrees well with the previous reports on Fe_3O_4 materials.[34,35] The discharge and charge capacities of the composite based on the total mass are 1423 mA h g^{-1} and 902 mA h g^{-1} in the first cycle, respectively. The coulombic efficiency is about 63.4% for the first cycle and higher than 94% during cycling. The irreversible capacity loss mainly results from the formation of a solid electrolyte interface (SEI) at low voltage below 1 V.[35,36] The capacity loss is slightly larger than that reported previously[37] probably due to the redox reaction of oxygen-containing functional groups on graphene sheets.[38,39]

The cyclic performance of the electrode is shown in Fig. 3b. The electrode was initially activated at the current density of 100 mA g^{-1} for 3 cycles, and then cycled at the current density of 500 mA g^{-1} for 100 cycles. The Fe_3O_4/GNS composite prepared without PVP was also measured as a comparison. Both of them could deliver a capacity of ~880 mA h g^{-1} at the current density of 500 mA g^{-1} after activation. However, the capacity of Fe_3O_4/GNS decreases rapidly to 430 mA h g^{-1} after the first 40 cycles and then stabilized afterward. In contrast, the Fe_3O_4/GNS–PVP showes excellent cycling stability with the capacity of 892 mA h g^{-1} after 100 cycles. The good cycling stability of Fe_3O_4/GNS–PVP is mainly due to the alleviation of the aggregation and pulverization in favor of the uniformly dispersing and larger porosity of the Fe_3O_4 particles on graphene.[40,41]

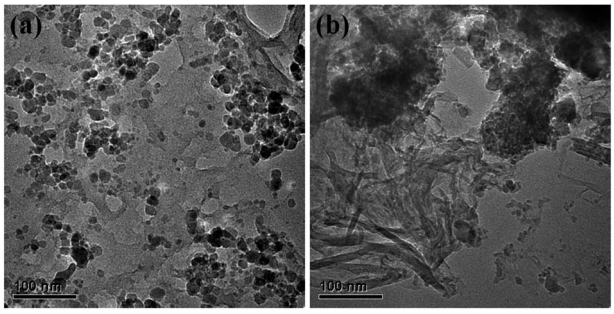

Fig. 2 (a) The TEM image of Fe_3O_4/GNS–PVP; (b) TEM image of Fe_3O_4/GNS.

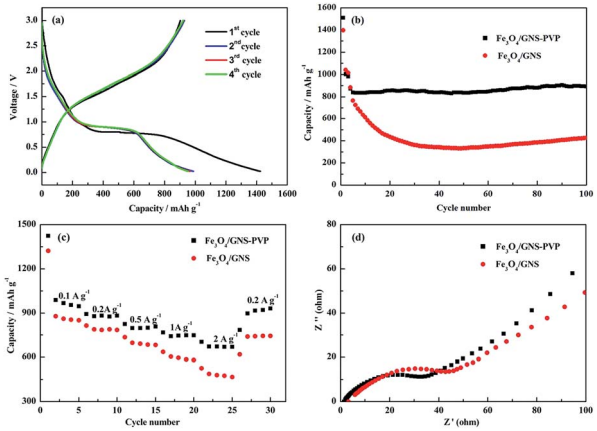

Fig. 3 (a) The discharge–charge curves of Fe_3O_4/GNS–PVP at the current density of 100 mA g^{-1}; (b) the cycling performance of Fe_3O_4/GNS–PVP and Fe_3O_4/GNS at the current density of 500 mA g^{-1}; (c) the reversible capacity of Fe_3O_4/GNS–PVP and Fe_3O_4/GNS at variation current densities; (d) the Nyquist plot of impedance spectra of Fe_3O_4/GNS–PVP and Fe_3O_4/GNS.

The Fe_3O_4/GNS–PVP composite also exhibits excellent rate capability. The reversible capacities of Fe_3O_4/GNS–PVP and Fe_3O_4/GNS at various current densities are shown in Fig. 3c. The Fe_3O_4/GNS–PVP could deliver a reversible capacity of 672 mA h g^{-1} even at the current density of 2 A g^{-1}. As a comparison, Fe_3O_4/GNS could only deliver the capacity of 488 mA h g^{-1} at the same condition. Note that the capacity of Fe_3O_4/GNS–PVP can recover to 895 mA h g^{-1} when the current density returns to 0.2 A g^{-1} after 25 cycles at different current densities even up to 2 A g^{-1}.

In order to further clarify the excellent lithium storage properties of Fe_3O_4/GNS–PVP, Raman spectrum was conducted to study the interaction of the two species in the composites (Fig. 4). For Fe_3O_4/GNS–PVP and Fe_3O_4/GNS, broad weak bands centered at around 678 cm^{-1} are observed, corresponding to the A1g mode of Fe_3O_4. This is in accordance with the results of XRD. Meanwhile, two obvious peaks of Fe_3O_4/GNS–PVP at 1342 and 1596 cm^{-1} are attributed to the fundamental D and G bands of carbon,[42,43] indicating the existence of graphene. D band is ascribed to defects such as the density of impurity, disordered carbon and oxygen-containing functional groups on graphene while the G band corresponds to in-plane stretching of ordered sp2 bonded carbon atoms. Compared to Fe_3O_4/GNS, a significant decrease in the intensity of the D band relative to the G band is observed when PVP was added. The decreasing in the intensity of the I_D/I_G indicated a lower degree of disorder within the GNS structure and the higher degree of reduction of GO. Notably, a G band shifting is observed from 1601 cm^{-1}

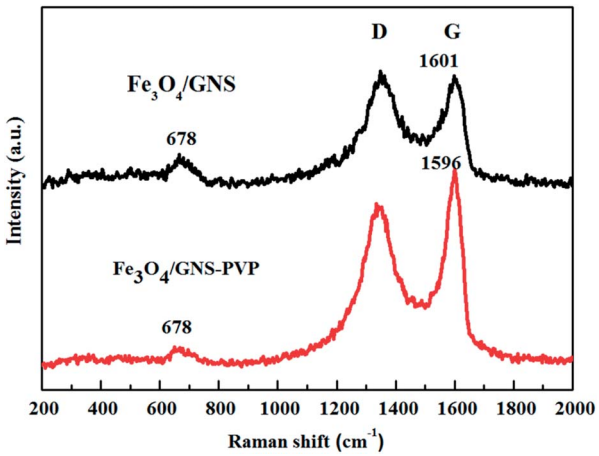

Fig. 4 Raman spectra of Fe_3O_4/GNS and Fe_3O_4/GNS–PVP.

(Fe_3O_4/GNS) to 1596 cm^{-1} (Fe_3O_4/GNS–PVP). It was reported that the G band shifting in carbon-based composites relates to the charge transfer between the carbon and other compounds present.[44,45] Therefore, it may indicate more charge of Fe_3O_4/GNS–PVP transferred from Fe_3O_4 to graphene, which will lead to easier bond breaking of Fe–O. It may be the key mechanism for the enhanced rate performance of Fe_3O_4/GNS–PVP over Fe_3O_4/GNS.

It should be noted that the two composites were very similar except the assistance of PVP during the synthesis process (PVP was washed away before sintering). For example, the BET specific surface area values and pore size distribution of both samples are comparable (40.6 m^2 g^{-1}, average BJH desorption pore diameter 8.6 nm for Fe_3O_4/GNS–PVP; 57.8 m^2 g^{-1}, average BJH desorption pore diameter 5.3 nm for Fe_3O_4/GNS, Fig S2†). The average crystallite size of Fe_3O_4 particles in the Fe_3O_4/GNS–PVP and Fe_3O_4/GNS composites are approximately 23 nm and 30 nm according to the Scherrer's formula based on the (311) peak (Fig. S1a†). Thus it is reasonable to assume that there is an interaction between Fe_3O_4 and GNS resulted from the assistance of PVP. Moreover, size effect may also contribute to the electrochemical differences in this study. According to previously reported result,[46] the aggregates of the primary particles without PVP have a bad influence on the electrochemical performances of Fe_3O_4 electrode. EIS results (Fig 3d) showed that the charge transfer resistance of Fe_3O_4/GNS electrode is as high as 61 Ω, while that of the Fe_3O_4/GNS–PVP is only about 43 Ω. The R_{CT} of Fe_3O_4/GNS is about 1.5 times larger than that of Fe_3O_4/GNS–PVP, suggesting that composites with well dispersed particles on graphene have good interfaces for charge transfer. This was in accordance with the results of Raman measurements.

In summary, we have synthesized a nanosized Fe_3O_4/GNS–PVP composite with excellent lithium storage properties. The superior electrochemical performance was attributed to the good dispersion of Fe_3O_4 and GNS, and the interaction between Fe_3O_4 and GNS. We also found the same phenomena on other transition metal oxide and graphene composites which showed enhanced electrochemical performance. However, more experimental evidence and direct characterization are highly desirable to elucidate this interaction between Fe_3O_4 and GNS. Further study is underway in our lab along this direction.

The authors gratefully acknowledge the financial support from the Key Project of NSFC (U1305246, 21321062) and the Major Project funded by Xiamen city (3502Z20121002).

Notes and references

1 L. M. Lang and Z. Xu, *ACS Appl. Mater. Interfaces*, 2013, **5**, 1698.
2 L. Li, T. T. Wang, L. Y. Zhang, Z. M. Su, C. G. Wang and R. S. Wang, *Chem. – Eur. J.*, 2012, **18**, 11417.
3 Y. Zhao, J. X. Li, C. X. Wu, Y. H. Ding and L. H. Guan, *ChemPlusChem*, 2012, **77**, 748.
4 Y. D. Huang, Z. F. Dong, D. Z. Jia, Z. P. Guo and W. I. Cho, *Electrochim. Acta*, 2011, **56**, 9233.
5 W. D. Zhang, X. Y. Wang, H. H. Zhou, J. T. Chen and X. X. Zhang, *J. Alloys Compd.*, 2012, **521**, 39.
6 L. Lu, J. Z. Wang, X. W. Gao, X. B. Zhu and H. K. Liu, *J. Nanosci. Nanotechnol.*, 2012, **12**, 1246.
7 Q. M. Zhang, Z. C. Shi, Y. F. Deng, J. Zheng, G. C. Liu and G. H. Chen, *J. Power Sources*, 2012, **197**, 305.
8 Q. Y. Hao, D. N. Lei, X. M. Yin, M. Zhang, S. Liu, Q. H. Li, L. B. Chen and T. H. Wang, *J. Solid State Electrochem.*, 2011, **15**, 2563.
9 J. C. Charlier, P. Eklund, J. Zhu and A. Ferrari, *Carbon Nanotubes: Advanced Topics in the Synthesis, Structure, Properties and Applications*, Springer, 2008, p. 673
10 C. Lee, X. Wei, J. W. Kysar and J. Hone, *Science*, 2008, **321**, 385.
11 A. Peigney, C. Laurent, E. Flahaut, R. Bacsa and A. Rousset, *Carbon*, 2001, **39**, 507.
12 Z. S. Wu, W. Ren, L. Wen, L. Gao, J. Zhao, Z. Chen, G. Zhou, F. Li and H. M. Cheng, *ACS Nano*, 2010, **4**, 3187.
13 X. Zhu, Y. Zhu, S. Murali, M. D. Stoller and R. S. Ruoff, *ACS Nano*, 2011, **5**, 3333.
14 Z. S. Wu, W. Ren, D. W. Wang, F. Li, B. Liu and H. M. Cheng, *ACS Nano*, 2010, **4**, 5835.
15 D. Chen, G. Ji, Y. Ma, J. Y. Lee and J. Lu, *ACS Appl. Mater. Interface*, 2011, **3**, 3078.
16 G. Zhou, D. W. Wang, F. Li, L. Zhang, N. Li, Z. S. Wu, L. Wen, G. Q. Lu and H. M. Cheng, *Chem. Mater.*, 2010, **22**, 5306.
17 Y. Dong, R. Ma, M. Hu, H. Cheng, Q. Yang, Y. Y. Li and J. A. Zapien, *Phys. Chem. Chem. Phys.*, 2013, **15**(19), 7174.
18 Y. Chen, B. Song, L. Lu and J. Xue, *Nanoscale*, 2013, **5**, 6797.
19 J. Su, M. Cao, L. Ren and C. Hu, *J. Phys. Chem. C*, 2011, **115**, 14469.
20 Y. Chen, H. Xia, L. Lu and J. Xue, *J. Mater. Chem.*, 2012, **22**, 5006.
21 Q. Q. Xiong, J. P. Tu, Y. Lu, J. Chen, Y. X. Yu, Y. Q. Qiao, X. L. Wang and C. D. Gu, *J. Phys. Chem. C*, 2012, **116**, 6495.
22 Z. Xiao, Y. Xia, Z. Ren, Z. Liu, G. Xu, C. Chao, X. Li, G. Shen and G. Han, *J. Mater. Chem.*, 2012, **22**, 20566.
23 Y. He, L. Huang, J. S. Cai, X. M. Zheng and S. G. Sun, *Electrochim. Acta*, 2010, **55**, 1140.

24 H. L. Liu, S. P. Ko, J. H. Wu, M. H. Jung, J. H. Min, J. H. Lee, B. H. An and Y. K. Kim, *J. Magn. Magn. Mater.*, 2007, **310**, e815.
25 H. Y. Lee, S. H. Lee, C. Xu, J. Xie, J. H. Lee, B. Wu, A. L. Koh, X. Wang, R. Sinclair and S. X. Wang, *Nanotechnology*, 2008, **19**, 165101.
26 I. Pardiñas-Blanco, C. E. Hoppe, Y. Piñeiro-Redondo, M. A. López-Quintela and J. Rivas, *Langmuir*, 2008, **24**, 983.
27 H. Tsunoyama, H. Sakurai, Y. Negishi and T. Tsukuda, *J. Am. Chem. Soc.*, 2005, **127**, 9374.
28 S. Guo, S. Dong and E. Wang, *ACS Nano*, 2009, **4**, 547.
29 J. Shen, X. Yin, D. Karpuzov and N. Semagina, *Catal. Sci. Technol.*, 2013, **3**, 208.
30 Y. Cui, X. Y. Lai, L. Li, Z. D. Hu, S. Wang, J. E. Halpert, R. B. Yu and D. Wang, *ChemPhysChem*, 2012, **13**, 2610.
31 M. Tsuji, K. Ikedo, M. Matsunaga and K. Uto, *CrystEngComm*, 2012, **14**, 3411.
32 H. L. Liu, P. Hou and J. H. Wu, *J. Mater. Res.*, 2011, **26**, 2040.
33 P. C. Lian, X. F. Zhu, H. F. Xiang, Z. Li, W. S. Yang and H. H. Wang, *Electrochim. Acta*, 2010, **56**, 834.
34 Y. Wu, Y. Wei, J. Wang, K. Jiang and S. Fan, *Nano Lett.*, 2013, **13**, 818.
35 Y. Dong, M. Hu, R. Ma, H. Cheng, S. Yang, Y. Y. Li and J. A. Zapien, *CrystEngComm*, 2013, **15**, 1324.
36 R. Wang, C. Xu, J. Sun, L. Gao and C. Lin, *J. Mater. Chem. A*, 2013, **1**, 1794.
37 Y. Ma, C. Zhang, G. Ji and J. Y. Lee, *J. Mater. Chem.*, 2012, **22**, 7845.
38 M. Zhang and M. Jia, *J. Alloys Compd*, 2013, **551**, 53.
39 B. Li, H. Cao, J. Shao, M. Qu and J. H. Warner, *J. Mater. Chem.*, 2011, **21**, 5069.
40 Z. Xiao, Y. Xia, Z. H. Ren, Z. Y. Liu, G. Xu, C. Y. Chao, X. Li, G. Shen and G. R. Han, *J. Mater. Chem.*, 2012, **22**, 20566.
41 J. Zhang, Y. Yao, T. Huang and A. Yu, *Electrochim. Acta*, 2012, **78**, 502.
42 S. Stankovich, D. A. Dikin, R. D. Piner, K. A. Kohlhaas, A. Kleinhammes, Y. Jia, Y. Wu, S. T. Nguyen and R. S. Ruoff, *Carbon*, 2007, **45**, 1558.
43 V. C. Tung, M. J. Allen, Y. Yang and R. B. Kaner, *Nat. Nanotechnol.*, 2008, **4**, 25.
44 A. M. Rao, P. C. Eklund, S. Bandow, A. Thess and R. E. Smalley, *Nature*, 1997, **388**, 257.
45 R. Kitaura, N. Imazu, K. Kobayashi and H. Shinohara, *Nano Lett.*, 2008, **8**, 693.
46 S. H. Lee, S. H. Yu, J. E. Lee, A. Jin, D. J. Lee, N. Lee, H. Jo, K. Shin, T. Y. Ahn, Y. W. Kim, H. Choe, Y. E. Sung and T. Hyeon, *Nano Lett.*, 2013, **13**(9), 4249.

